



# Long-Term Global Land Surface Satellite (GLASS) Fractional Vegetation Cover Product Derived From MODIS and AVHRR Data

Kun Jia , Linqing Yang, Shunlin Liang , Fellow, IEEE, Zhiqiang Xiao , Xiang Zhao, Yunjun Yao , Xiaotong Zhang , Bo Jiang , and Duanyang Liu

## I. INTRODUCTION

**Abstract**—Long-term global land surface fractional vegetation cover (FVC) data are essential for global climate modeling, earth surface process simulations, and related applications. However, high quality and long time series global FVC products remain scarce, although several FVC products have been generated using remote sensing data. This study aims to use the previously proposed Global Land Surface Satellite (GLASS) FVC product from Moderate Resolution Imaging Spectroradiometer (MODIS) data (denoted as GLASS-MODIS FVC) to generate a long term GLASS FVC product from advanced very high resolution radiometer (AVHRR) data (denoted as GLASS-AVHRR FVC) back to year 1981. The GLASS-AVHRR FVC algorithm adopted the multivariate adaptive regression splines method, which was trained using samples extracted from the GLASS-MODIS FVC product and the corresponding red and near-infrared band reflectances of the preprocessed AVHRR reflectance data from 2003 over the global sampling locations. The GLASS-AVHRR FVC product has a temporal resolution of eight days and a spatial resolution of 0.05°. Through comparison of the GLASS-AVHRR and GLASS-MODIS FVC products from 2013, good temporal and spatial consistencies were observed, which confirmed the reliability of the GLASS-AVHRR FVC product. Furthermore, direct validation using field FVC measurement based reference data indicated that the performance of the GLASS-AVHRR FVC product ( $R^2 = 0.834$ , RMSE = 0.145) was slightly superior to that of the popular long term GEOV1 FVC product ( $R^2 = 0.799$ , RMSE = 0.174).

**Index Terms**—Advanced very high resolution radiometer (AVHRR), climate change, fractional vegetation cover (FVC), global land surface, long time series data .

Manuscript received March 30, 2018; revised May 23, 2018 and July 2, 2018; accepted July 5, 2018. Date of publication July 22, 2018; date of current version March 4, 2019. This work was supported in part by the National Key Research and Development Program of China under Grant 2016YFA0600103 and 2016YFB0501404, and the National Natural Science Foundation of China under Grant 41671332. (K. Jia and L. Yang contributed equally to this work.) (Corresponding author: Kun Jia.)

K. Jia, L. Yang, Z. Xiao, X. Zhao, Y. Yao, X. Zhang, B. Jiang, and D. Liu are with the State Key Laboratory of Remote Sensing Science, Faculty of Geographical Science, Beijing Normal University, Beijing 100875, China and also the Beijing Engineering Research Center for Global Land Remote Sensing Products, Faculty of Geographical Science, Beijing Normal University, Beijing 100875, China (e-mail: jiakun@bnu.edu.cn; linqingyang@mail.bnu.edu.cn; zhqxiao@bnu.edu.cn; zhaoxiang@bnu.edu.cn; boyyunjun@163.com; xtngzhang@bnu.edu.cn; bojiang@bnu.edu.cn; 201721170045@mail.bnu.edu.cn).

S. Liang is with the Department of Geographical Sciences, University of Maryland, College Park, MD 20742 USA and also the School of Remote Sensing Information Engineering, Wuhan University, China (e-mail: sliang@umd.edu).

Color versions of one or more of the figures in this paper are available online at <http://ieeexplore.ieee.org>.

Digital Object Identifier 10.1109/JSTARS.2018.2854293

GLOBAL climate change has led to a series of problems such as lack of fresh water, desertification, food shortages, and biodiversity losses [1]–[4]. Vegetation, as the core composition of terrestrial ecosystems, is a sensitive indicator of climate change and influences climate change by influencing the energy, water, and carbon cycles [5]–[8]. Fractional vegetation cover (FVC), generally defined as the fraction of green vegetation seen from nadir, is an important variable for characterizing land surface vegetation conditions [9]–[12]. FVC is also a key biophysical parameter for studying the atmosphere, land surface, hydrosphere, and biosphere as well as their interactions [16], [17]. The interactions between climate change and vegetation as well as the interactions among each earth sphere are processes of long term effects. Therefore, a long term and global scale FVC data set is of great significance for land surface processes and climate change studies as well as its extensive applications in monitoring agriculture, forestry, disaster risks, and drought [1], [11], [18]–[21].

Remote sensing provides the effective and comprehensive means for long term and global scale FVC estimation because of its ability to quickly and repeatedly collect information at a global scale [13], [22]. The commonly used methods for FVC estimation using remote sensing data mainly include empirical methods, pixel unmixing models, and physical methods [23]–[26]. The empirical methods are based on the linear or nonlinear statistical relationships between FVC and vegetation indices or spectral reflectance of specific bands [25]. The empirical methods are computationally efficient, but the empirical relationships usually vary with different vegetation types and regions. Therefore, the empirical methods are difficult to use for FVC estimation at continental or global scales because of the complexity of land surfaces. The pixel unmixing models assume that each pixel is comprised of several components and consider the fraction of vegetation compositions as the FVC of each pixel [24], [28], [29]. The dimidiate pixel model is a widely used pixel unmixing model that assumes pixels are only comprised of vegetation and nonvegetation compositions [19], [24], [30]. However, it is difficult to determine the endmember and the spectral responses of endmembers for pixel unmixing models over larger extents, which limits the application of pixel unmixing models to estimate FVC globally. The physical methods

TABLE I  
SEVERAL COMMONLY USED REMOTE SENSING DATA BASED LARGE SCALE FVC PRODUCTS

Source/Project name	Sensor	estimation methods	Available time	Temporal resolution	Spatial coverage	Spatial resolution	Reference
CNES/POLDER	POLDER	Machine learning methods	1996-1997, 2003	10 days	Global	6 km	[1]
FP5/CYCLOPES	SPOT VGT	Machine learning methods	1998-2007	10 days	Global	1 km	[13]
ESA/MERIS	MERIS	Machine learning methods	2002-2012	Month/10 days	Global	300 m	[14]
EUMETSAT/LSA SAF	SEVIRI	The dimidiate pixel model	2005-now	Daily	Europe, Africa, South American	3 km	[15]
GEOV1	AVHRR/SPOT VGT	Machine learning methods	1981-now	10 days	Global	1981-2000 (0.05°) 1999-now (1 km)	[9]
GLASS	MODIS	Machine learning methods	2000-now	8 days	Global	0.5 km	[11, 27]

are based on canopy radiative transfer models that simulate the physical relationships between vegetation canopy spectral reflectance and FVC. Due to the complexity of physical models, machine learning methods are usually used to simplify the estimation of FVC by training with simulated reflectance databases from physical models [1], [9], [31]. The machine learning methods are computationally efficient, robust to noisy data, and can approximate multivariate nonlinear relationships, which make them popular choices for large-scale FVC estimation [9], [32]–[34]. One key issue for machine learning methods is to generate a comprehensive learning data set for the training process.

Furthermore, several large scale FVC products have been generated using coarse resolution remote sensing data (see Table I). The POLDER FVC product is generated using neural networks (NNs) based on the simulations from the Kuusk Model [1]. The MERIS and CYCLOPES FVC products are generated using NNs that are trained using learning data sets from simulations of the PROSPECT+SAIL model [13], [14]. By correcting the underestimation, the GEOV1 FVC product is an improved version of the CYCLOPES FVC product [9]. However, the accuracy validations of these FVC products are not satisfactory [35]–[37]. For example, the MERIS FVC product presents systematic underestimations of FVC values of approximately 0.1–0.2 compared to the SEVIRI FVC product over Europe and Africa [36]. The values of the CYCLOPES FVC product are larger than those of the SEVIRI FVC product by approximately 0.15 over the Sahel region in the year 2007, but the validation reports note that the values of the CYCLOPES FVC product are lower than those values of spatial aggregation from high spatial resolution SPOT data, thus the FVC products of SEVIRI, MERIS, and CYCLOPES all underestimate FVC to some extent [38]. The GEOV1 FVC product is generated by correcting the systematic underestimation of the CYCLOPES FVC product and is considered as being closer to the ground FVC estimates, which is considered to be the best global FVC product from SPOT VEGETATION data [35]. However, the GEOV1 FVC product presents visible missing data, especially at high latitudes in the northern hemisphere in winter time [11], [27]. For example, the GEOV1 FVC product presented visible missing data that were approximately 43.1% and 7.9% of the land surface pixels for January and July of year 2003, respectively [11]. The Global Land Surface Satellite (GLASS) FVC product from moderate resolution imaging spectroradiometer (MODIS) reflectance data (denoted as GLASS-MODIS FVC) is generated using the multivariate adaptive regression splines (MARS) method, whereas the training samples are generated from finer resolution remote

sensing data [11], [27]. The validation of the GLASS-MODIS FVC product presents a comparable accuracy with that of the GEOV1 FVC product, but the temporal and spatial continuities of the GLASS-MODIS FVC product are much better than those of the GEOV1 FVC product. Another important limitation regarding the existing FVC products is that a long term time series FVC product is lacking. Although the GEOV1 FVC product from advanced very high resolution radiometer (AVHRR) data can be backtracked to 1981, its accuracy is not clear due to lack of validation data. Therefore, a reliable and long-term time series global FVC product is not sufficient for supporting studies of long-term global climate change and land surface processes.

Therefore, the objective of this study is to develop a reliable FVC product from AVHRR reflectance data (denoted as GLASS-AVHRR FVC) that is in concert with the GLASS-MODIS FVC product to form a long-term time series global FVC product for supporting studies of global climate change and land surface processes. The GLASS-AVHRR FVC algorithm is based on the GLASS-MODIS FVC product to achieve continuity of FVC estimates from both AVHRR and MODIS data. First, training samples over global sampled locations are extracted from one year overlapped AVHRR reflectance data and GLASS-MODIS FVC product. Then, the samples are used for training MARS. The trained MARS is used to estimate time series global FVC from AVHRR reflectance data, and the performances of the FVC estimates are compared with GLASS-MODIS and GEOV1 FVC products.

## II. DATA AND PREPROCESSING

### A. GLASS-MODIS FVC Product

The GLASS FVC product was supported by China's National High Technology Research and Development Program, which was generated using the MARS method with training samples derived from global sampled Landsat data [11], [27]. The direct validation results indicated that the GLASS-MODIS FVC product (RMSE = 0.149) had comparable performances to those of the GEOV1 FVC product (RMSE = 0.166) based on the validation samples from the Validation of Land European Remote sensing Instruments (VALERI) sites. In addition, the GLASS-MODIS FVC product was spatially and temporally compared with the GEOV1 FVC product based on monthly averaged global FVC maps in 2003 and temporal FVC profiles over validation sites from 2000 to 2010. The comparison results indicated that the GLASS-MODIS FVC product presented good temporal and spatial continuities with no missing

data observed, whereas the GEOV1 FVC product presented visible missing data that were approximately 43.1% and 7.9% of the land surface pixels for January and July of year 2003 [11]. Thus, the GEOV1 FVC product was not suitable for generating the time series training samples for developing the GLASS-AVHRR FVC algorithm. Therefore, the GLASS-MODIS FVC product was the reliable choice and was selected for generating the time series training samples used to develop the GLASS-AVHRR FVC product. The temporal and spatial resolutions of GLASS-MODIS FVC were eight days and 0.5 km, respectively, with a sinusoidal grid projection. For spatial and temporal matching with AVHRR reflectance data, the GLASS-MODIS FVC data were reprojected to a spatial resolution of  $0.05^\circ$  with geographic projection.

### B. AVHRR Reflectance Data

The AVHRR land surface reflectance data were acquired from the AVH09 Surface Reflectance Product (Version 5) generated by the Land Long Term Data Record project, which aimed to produce a consistent long-term data set from AVHRR and MODIS instruments for global change and climate studies [39]. AVH09 was provided in HDF-EOS format and contained daily surface reflectance at a spatial resolution of  $0.05^\circ$  in a geographic projection. The AVHRR reflectance data used in this study included red ( $0.58\text{--}0.68\ \mu\text{m}$ , channel 1) and near-infrared (NIR,  $0.725\text{--}1.10\ \mu\text{m}$ , channel 2) spectral channels. The AVH09 reflectance data were already atmospherically corrected, as were Rayleigh scattering, ozone, water vapor, and aerosols.

To obtain high-quality AVHRR reflectance data, the temporally continuous vegetation indices-based land-surface reflectance reconstruction (referred to as VIRR) method [40] was used to detect and reconstruct the remaining cloudy or partially cloudy influenced pixels in the reflectance data. The daily AVHRR surface reflectance data were first aggregated into 8-day intervals using the constraint view angle, maximum value composite method [41] to maintain a temporal resolution consistent with the MODIS data. The 8-day AVHRR surface reflectance data then were used to calculate NDVI. Next, a penalized least-squares regression based on a three-dimensional discrete cosine transform developed by Garcia [42] was used to reconstruct continuous and smooth NDVI upper envelopes, and cloud-contaminated values were detected using the time series NDVI and their upper envelopes. Finally, the high-quality surface reflectance data along with continuous and smooth NDVI upper envelopes were used to reconstruct surface reflectance time series by minimizing cost functions of models fitted to surface reflectance data [40]. The reconstructed 8-day temporal resolution AVHRR reflectance data using the VIRR method would be used to generate the GLASS-AVHRR FVC product.

## III. METHODOLOGY

This study extended the MARS method for GLASS-MODIS FVC product generation to estimate FVC from AVHRR reflectance data (see Fig. 1). First, the AVHRR reflectance and GLASS-MODIS FVC data for year 2003 were preprocessed for spatial and temporal matching using geographic projection.

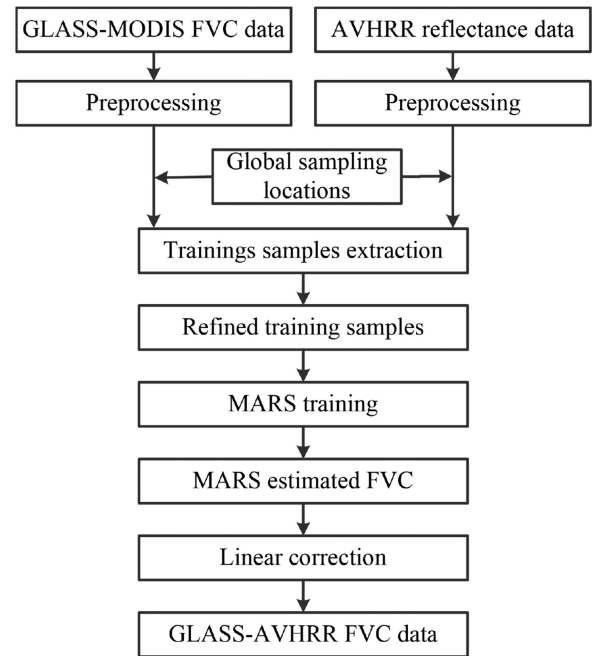


Fig. 1. Flowchart of the method used to develop GLASS-AVHRR FVC product.

Then, the training samples were extracted over the global sampling locations and further refined. Next, the MARS was trained with the refined training samples and used to estimate FVC from the preprocessed AVHRR reflectance data. Finally, the estimated FVC from AVHRR data were linearly corrected based on GLASS-MODIS FVC to obtain consistent FVC data with GLASS-MODIS FVC.

### A. Training Samples Generation

The training samples with spatial and temporal representativeness were essential for modeling the relationships between FVC and AVHRR reflectance data using the MARS method. In this study, the training samples were generated over the BELMANIP2.1 sites [9], [43] to enhance the spatial representativeness. The BELMANIP2.1 sites contained 445 sites located in relatively flat and homogeneous areas (at a kilometeric resolution over  $10 \times 10\ \text{km}^2$  domains) with representative global distributions of vegetation types and conditions [9]. The entirety of year 2003 was selected to represent the seasonal variability of vegetation and to enhance the temporal representativeness of the training samples. The pixel values of the GLASS-MODIS FVC data and the red and NIR band reflectances of the preprocessed AVHRR data were extracted over each of the global sampling locations. To refine the original extracted sampling data for consistency and remove abnormal samples, the sampling FVC values were plotted against NDVI values calculated from AVHRR reflectance. Then, for each group of NDVI values (20 classes over the  $[0, 1]$  domain of variation), the cases with FVC values lower than the 5% percentile or higher than the 95% percentile were removed from the training samples (see Fig. 2). This process could be used to effectively remove abnor-



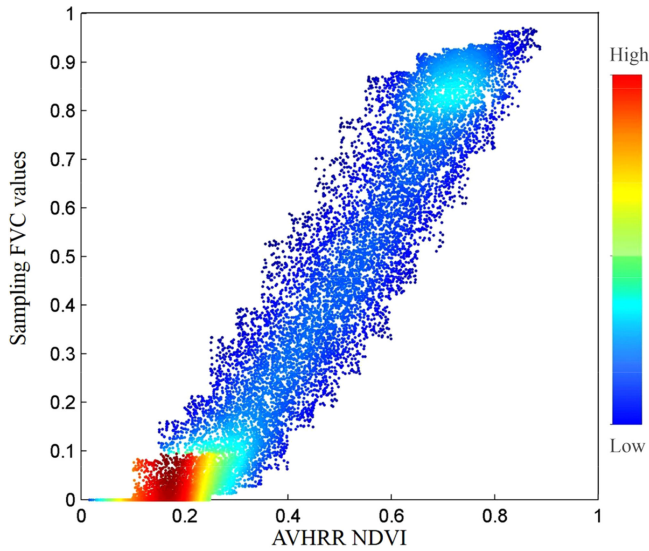


Fig. 2. Scatter plots between AVHRR NDVI and the sampling FVC values from GLASS-MODIS FVC product, and the density map presents the densities of the selected samples.

mal samples because FVC usually presented approximate linear relationship with NDVI and then avoid influences in the training of MARS caused by inaccurate samples. Finally, 17 394 refined cases with consistent AVHRR reflectances paired with GLASS-MODIS FVC values were confirmed as the training samples for the MARS method.

### B. Training of MARS

MARS is a nonparametric and multivariate regression analysis model that has been demonstrated to have satisfactory performance for FVC estimation from MODIS and Landsat reflectance data [27], [34], [44]. Therefore, MARS was also selected to develop the GLASS-AVHRR FVC product given its computational efficiency and satisfactory accuracy. MARS was capable of modeling complex nonlinear relationships among variables by fitting piecewise linear regressions. MARS built models of a set of basis functions [34], [44]:

$$f(x) = a_0 + \sum_{m=1}^M a_m B_m(x). \quad (1)$$

A basis function is the tensor product of the spline functions:

$$B_m(x) = \prod_{k=1}^{K_m} [S_{k,m}(x(k,m) - t_{k,m})] \quad (2)$$

where  $a_0$  is the coefficient of the constant basis function;  $a_m$  are the coefficients of the model, which are estimated to yield the best fit to the training data;  $B_m(x)$  are the basis functions, for which  $x(k,m)$  is the index of the independent variable used in the  $m$ th term of the  $k$ th product;  $M$  is the number of basis functions;  $K_m$  is the number of splits that generate the  $m$ th basis function;  $S_{k,m}$  takes values of either 1 or  $-1$  and indicates the right/left sense of the associated step function;  $x(k,m)$

is the independent variable label; and  $t_{k,m}$  indicates the knot locations.

The optimal MARS model was determined by a two-stage process. First, MARS constructed a very large number of basis functions to fit the training data, where variables could interact with each other. Then, the basis functions were deleted in the order of least importance using the generalized cross-validation criterion [45]. Additional details regarding the MARS model building process can be found in the work of Friedman *et al.* [45]. In this study, the MARS model inputs included the reflectances of red and NIR bands from the preprocessed AVHRR data, and the output was the corresponding FVC.

### C. MARS Estimated FVC From AVHRR Data

Some reflectances of nonvegetation pixels such as water body and desert pixels might influence the prediction accuracy of the MARS model and result in abnormal FVC estimates. Therefore, it was a good strategy to first identify these nonvegetation pixels and set their FVC values to zero instead of estimating their FVC using the trained MARS model. NDVI was always used to describe vegetation conditions and estimate FVC based on empirical relationships between FVC and NDVI [19], [24] and is thus a good choice to identify nonvegetation pixels. In this study, a conservative NDVI threshold value of 0.05 was used to determine the nonvegetation pixels, which was also a value used as bare soil NDVI in the dimidiate pixel model for FVC estimation from AVHRR data [20]. Thus, FVC values for the identified nonvegetation pixels would be set to zero, and those for other pixels would be estimated using the trained MARS model.

### D. Linear Correction of the MARS Estimated FVC

Due to the differences of MODIS and AVHRR sensors and the differences of preprocessing of the MODIS and AVHRR reflectance data, the FVC estimates from AVHRR data and MODIS data might differ as well, which was inconvenient for applications of the long-term FVC product. Therefore, to generate consistent FVC estimates from AVHRR and MODIS data, the MARS estimated FVC from AVHRR data were linearly corrected based on the aggregated  $0.05^\circ$  spatial resolution GLASS-MODIS FVC data. Specifically, each pixel's linear regression equation was established using the MARS estimated FVC from AVHRR data and the GLASS-MODIS FVC data from the overlapped years of 2000 to 2015. Then, the MARS estimated FVC data from 1981 to 2015 were corrected using the established linear regression equations at each pixel. Finally, the linearly corrected FVC data from AVHRR data would be denoted as the GLASS-AVHRR FVC product.

### E. Accuracy Assessment and Product Comparison

The direct accuracy assessment of coarse resolution FVC estimates always uses high spatial resolution remote sensing data to scale the ground measurements up to the low spatial resolution for comparison [46]. The validation samples based on ground FVC measurements were acquired from the VALERI sites, the

TABLE II  
CHARACTERISTICS OF THE SITES SELECTED FOR ACCURACY ASSESSMENT

Site Name	Lat (°)	Lon (°)	Land cover	DOY	Year	FVC
Barrax	39.06	-2.10	Croplands	193	2003	0.236
Camerons	-32.60	116.25	wooded savannas	63	2004	0.414
Chilbolton	51.16	-1.43	Deciduous needleleaf forest	166	2006	0.647
Counami	5.35	-53.24	Evergreen needleleaf Forest	269	2001	0.838
Counami	5.35	-53.24	Evergreen needleleaf Forest	286	2002	0.858
Demmin	53.89	13.21	Cropland	164	2004	0.586
Donga	9.77	1.78	Savannas	172	2005	0.420
Fundulea	44.41	26.58	Cropland	128	2001	0.341
Fundulea	44.41	26.58	Cropland	144	2002	0.374
Fundulea	44.41	26.59	Cropland	144	2003	0.319
Gilching	48.08	11.32	Mixed forest	199	2002	0.676
Gnangara	-31.53	115.88	savannas	61	2004	0.221
Gourma	15.32	-1.55	Grasslands	244	2000	0.236
Gourma	15.32	-1.55	Grasslands	275	2001	0.126
Haouz	31.66	-7.60	Croplands	71	2003	0.248
Hirsikangas	62.64	27.01	Mixed Forest	226	2003	0.644
Hirsikangas	62.64	27.01	Mixed Forest	190	2004	0.537
Hirsikangas	62.64	27.01	Mixed Forest	159	2005	0.442
Hombori	15.33	-1.48	Grasslands	242	2002	0.200
Jarvselja	58.29	27.29	Mixed Forest	188	2000	0.705
Jarvselja	58.30	27.26	Mixed Forest	165	2001	0.783
Jarvselja	58.30	27.26	Mixed Forest	178	2002	0.793
Jarvselja	58.30	27.26	Mixed Forest	208	2003	0.803
Jarvselja	58.30	27.26	Mixed Forest	180	2005	0.842
Jarvselja	58.30	27.26	Mixed Forest	112	2007	0.535
Jarvselja	58.30	27.26	Mixed Forest	199	2007	0.731
Laprida	-36.99	-60.55	Grasslands	311	2001	0.722
Laprida	-36.99	-60.55	Grasslands	292	2002	0.534
Larose	45.38	-75.22	Mixed forest	219	2003	0.847
Le Larzac	43.94	3.12	Wooded savannas	183	2002	0.300
Les Alpilles	43.81	4.71	Cropland	204	2002	0.349
Plan-de-Dieu	44.20	4.95	Cropland	189	2004	0.172
Puechabon	43.72	3.65	Mixed Forest	164	2001	0.540
Rovaniemi	66.46	25.35	Cropland	161	2004	0.423
Rovaniemi	66.46	25.35	Cropland	166	2005	0.497
Sonian forest	50.77	4.41	Mixed Forest	174	2004	0.903
Concepcion	-37.47	-73.47	Mixed forest	9	2003	0.455
Hyytiälä	61.85	24.31	Evergreen Needleleaf forest	188	2008	0.461
Sud_Ouest	43.51	1.24	Cropland	189	2002	0.352
Turco	-18.24	-68.18	Open Shrubland	208	2001	0.106
Turco	-18.24	-68.19	Open Shrubland	240	2002	0.020
Turco	-18.24	-68.19	Open Shrubland	105	2003	0.044
Wankama	13.64	2.64	Grasslands	174	2005	0.036
Zhang Bei	41.28	114.69	Grasslands	221	2002	0.353

\* DOY: Day of Year; FVC: Fractional vegetation cover.

aim of which was to provide high spatial resolution maps of biophysical variables estimated from ground measurements to validate products derived from satellite observations (accessed at <http://w3.avignon.inra.fr/valeri/>) [35]. The locations of the eligible validation sites, measurement information, and FVC values are provided in Table II. The FVC values (meaning values from 3 km × 3 km site areas) of the sites were derived from high-resolution remote sensing data based on an empirical transfer function between the field FVC measurements and radiometric signal. Although the area of the sites was smaller than one AVHRR pixel, considering the homogeneity around the sites, the FVC values could represent the FVC level of one AVHRR pixel

to some extent. Therefore, the FVC values over these sites were used to compare the performances of the GLASS-AVHRR and GEOV1 FVC products. The validation sites contained various land cover types such as forest, grassland, and cropland. Therefore, although the 44 validation samples were not so large, they were representative of the typical vegetation types, and the performances of the two FVC products would be demonstrated. The GLASS-AVHRR and GEOV1 FVC products were linearly interpolated to the FVC acquisition dates over the validation sites.

An intercomparison with existing FVC products was another important way to confirm the reliability of the GLASS-AVHRR FVC product [11], [35]. The GLASS-AVHRR FVC product for year 2013 was spatially and temporally compared with the GLASS-MODIS FVC product. For the purposes of this study, which were to extend the GLASS-MODIS FVC algorithm and to prolong the temporal coverage of the GLASS-MODIS FVC product, the comparison of the two FVC products could be considered as an independent and direct validation of the GLASS-AVHRR FVC product. The only other existing long-term FVC product from GEOV1 was also selected for comparison with the performance of the GLASS-AVHRR FVC product. The monthly averaged global FVC maps in January and July, which represent two different vegetation growth seasons, were generated from different FVC products to compare the spatial consistency and spatial continuity. To compare the temporal consistency and temporal continuity of different FVC products, annual FVC temporal profiles at the sampling sites were also extracted for evaluation.

## IV. RESULTS AND ANALYSIS

### A. GLASS-AVHRR FVC Product

The monthly averaged global FVC maps from the GLASS-AVHRR and GLASS-MODIS FVC products were generated in January and July of 2013 to compare the two products (see Fig. 3). By visual observations, there was a good spatial agreement between the GLASS-AVHRR and GLASS-MODIS FVC products. That result indicated the good spatial consistency between the two FVC products. The distribution of FVC values from both products was consistent with the actual conditions of land cover distributions and seasonal variations. The tropical rain forest regions presented high FVC values, whereas the desert regions and glacier regions had FVC values of zero for the whole year. The temperate zone in the mid-high latitude regions of the Northern Hemisphere presented high FVC values in summer and low FVC values in winter, which was coincident with vegetation growth characteristics in these regions. These results confirmed that the GLASS-AVHRR FVC were consistent with GLASS-MODIS FVC, which could indicate the reliability of the GLASS-AVHRR FVC product. Furthermore, the global land surface FVC maps generated from the GLASS-AVHRR FVC product achieved good spatial continuity performance, and no missing data were observed. These results confirmed that pre-processing of AVHRR data could obtain continuous reflectance values and thus generate a spatially and temporally continued GLASS-AVHRR FVC product.

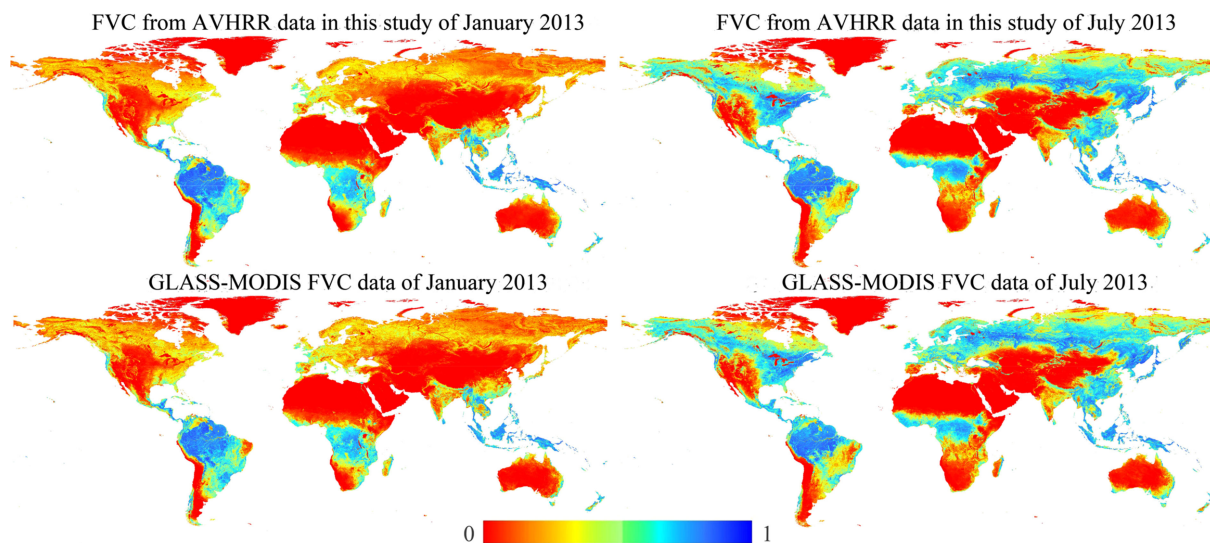


Fig. 3. Monthly averaged global FVC maps from the GLASS-AVHRR and GLASS-MODIS FVC products for January and July of 2013. The Antarctic Territories are not included in the map.

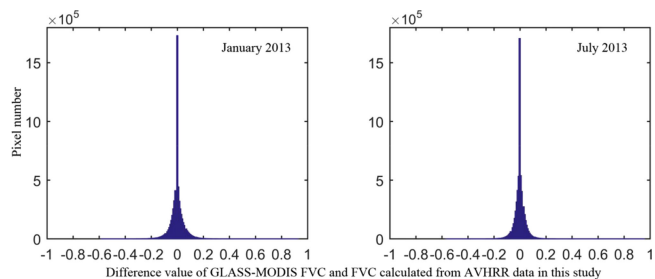


Fig. 4. Histograms of difference values between GLASS-MODIS and GLASS-AVHRR FVC products for January and July of 2013.

To quantitatively evaluate the performance of the GLASS-AVHRR FVC product, histograms of difference values between the GLASS-MODIS and GLASS-AVHRR FVC data in January and July of 2013 were generated for the land surface (see Fig. 4). The peak values were located around zero, which indicated very small differences between the two FVC products. Quantitatively, more than 97.96% of the difference values were located between  $-0.1$  and  $0.1$ , and more than 99.81% of the difference values were located between  $-0.2$  and  $0.2$ . These observations further confirmed that the differences between the two FVC products were small and indicated that the performance of the GLASS-AVHRR FVC product was satisfactory.

Fig. 5 provides the monthly averaged GLASS-AVHRR and GLASS-MODIS FVC maps over the Amazon River Basin for January and July of 2013 to show their detailed differences. Generally, the spatial distributions and the magnitudes of the two FVC products are highly consistent, which confirms their consistency. Furthermore, the two FVC products show high FVC values over most areas of the Amazon River Basin. In addition, the Amazon River Basin is characterized by a dry season and wet season. January belongs to the wet season, and July belongs to the dry season. Generally, the vegetation cover in July is greener than that in January in the central and eastern Amazon

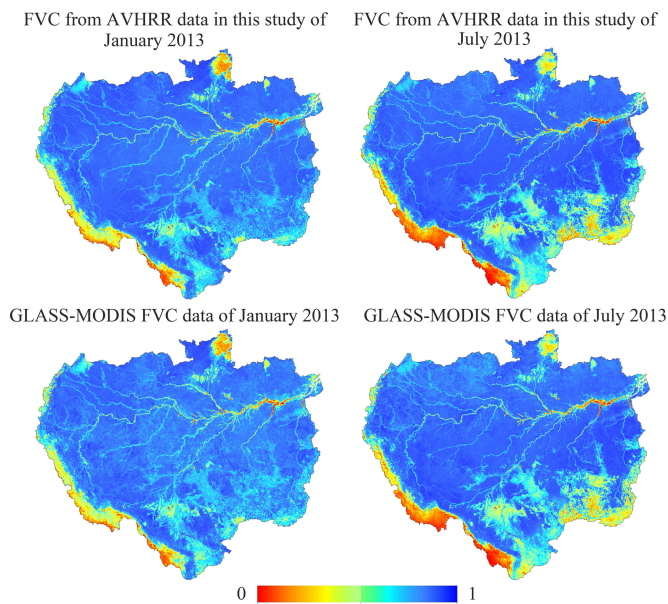


Fig. 5. Monthly averaged GLASS-AVHRR and GLASS-MODIS FVC maps over Amazon River Basin for January and July of 2013.

rainforests, which is consistent with the current research results [47], [48]. That is because sunlight may exert more influence than rainfall on rainforest phenology and productivity during the dry season [47]. These results confirmed that the GLASS-AVHRR FVC were consistent with GLASS-MODIS FVC and could reflect the actual vegetation cover conditions, which could indicate the reliability of the GLASS-AVHRR FVC product.

In total, 445 FVC temporal profiles at the pixels of each of the BELMANIP2.1 sites in the year of 2013 were generated to compare the temporal consistencies and continuities of the GLASS-AVHRR and GLASS-MODIS FVC products. Because of the limited space, several representative FVC temporal profiles, including woodland, shrubland, grassland, and



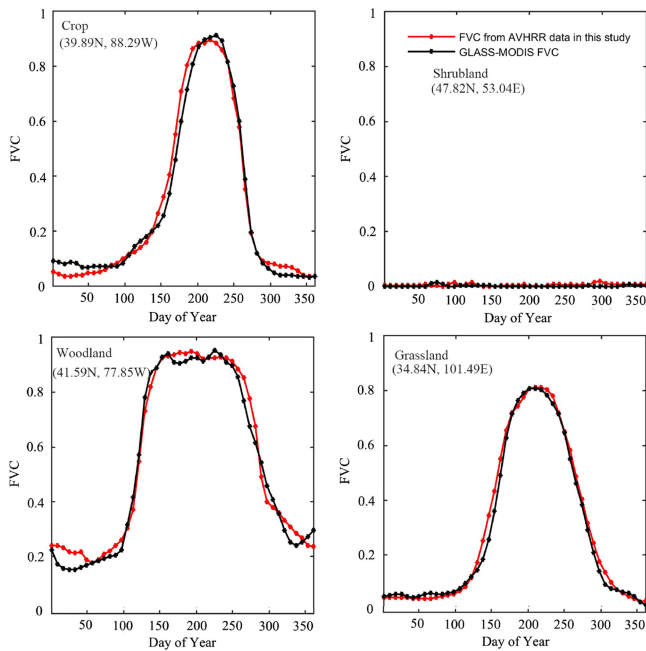


Fig. 6. Temporal profiles of the FVC from the GLASS-AVHRR and GLASS-MODIS FVC products over sampling sites for year 2013.

cropland, are shown in Fig. 6. The temporal profiles from the GLASS-AVHRR FVC product presented a similar magnitude and dynamic range as those derived from the GLASS-MODIS FVC product. There was also clear seasonality in different vegetation types in both products, which could clearly describe the vegetation growth characteristics. For example, in the cropland sites, the FVC rapidly increased with the rapid growth of crops, reached the peak value in the vigorous growth period, and finally decreased with the maturation and harvesting of the crops. In addition, the temporal profiles from the GLASS-AVHRR FVC product show some slight fluctuations. These slight fluctuations were inevitably affected by the atmosphere and could be effectively smoothed in specific applications of FVC using temporal filter methods such as the Savitzky–Golay filter method and locally adjusted cubic-spline capping method [49], [50]. Therefore, it could be confirmed that the temporal consistency of the two FVC products was good and further indicated the satisfactory performance of the GLASS-AVHRR FVC product.

Overall, the comparisons between the GLASS-AVHRR and GLASS-MODIS FVC products indicated that the FVC estimation algorithm was reliable and could generate long term, spatially and temporally continuous global FVC products from AVHRR data. These global FVC products would extend the GLASS-MODIS FVC product to the year 1981 and provide consistent and high-quality FVC estimates for related studies.

### B. Comparison With the GEOV1 FVC Product

Comparison with other existing FVC products is another important means to validate the performance of the proposed GLASS-AVHRR FVC product. The GEOV1 FVC from AVHRR data was spatially and temporally compared with the GLASS-AVHRR FVC product and was directly validated using

ground measurements based reference FVC data. The monthly averaged global FVC maps from the GLASS-AVHRR and GEOV1 FVC products in January and July of 1993 are presented in Fig. 7. The spatial consistency between the two FVC products was good in most regions of the land surface, which indicated the reasonability of the GLASS-AVHRR FVC product. There were more evident differences between the two FVC products in the equatorial region and the mid-high latitude regions of the Northern Hemisphere than in other regions for both January and July (see Fig. 7). Both FVC products presented good seasonality of FVC, which corresponded to the actual vegetation growth characteristics. In addition, a small number of missing data was observed for the GEOV1 FVC product, whereas there were no missing data for the GLASS-AVHRR FVC product. Therefore, the comparable spatial distributions of the two FVC products could indicate the reasonability of the GLASS-AVHRR FVC product and the good spatial continuities of the estimated FVC in this study.

The histograms of difference values between the GEOV1 and GLASS-AVHRR FVC products in January and July of 1993 are presented in Fig. 8. Meanwhile, the peak values were located around zero. However, compared to the comparison between FVC from the GLASS-AVHRR and GLASS-MODIS FVC products, a certain number of pixels showed larger differences between these two products, especially for the FVC estimates in July. There were many negative difference values, the main reason being that the GLASS-AVHRR FVC product presented obviously higher values than the GEOV1 FVC product in the tropical rainforest regions of equatorial regions, which was consistent with that seen in Fig. 7. The high FVC values of this study might be reasonable because of the thick perennial vegetation cover of the tropical rainforest. Quantitatively, approximately 69.0% of the difference values were located between  $-0.1$  and  $0.1$ , and approximately 90.7% of the difference values were located between  $-0.2$  and  $0.2$ . Therefore, although the two FVC products had similar spatial distributions, there were also certain differences between the two products in specific regions.

Fig. 9 provides the monthly averaged GLASS-AVHRR and GEOV1 FVC maps over the Amazon River Basin for January and July of 1993 to show their detailed differences. Generally, the spatial distributions and the magnitudes of the two FVC products were highly consistent. However, most of the FVC values of the GLASS-AVHRR FVC product are higher than those of the GEOV1 FVC product. Because of the high vegetation coverage in the Amazon Rainforest, the higher FVC values of the GLASS-AVHRR FVC may be reasonable. These results demonstrated that the spatial distributions of the GLASS-AVHRR and GEOV1 FVC products are comparable and that the GLASS-AVHRR FVC product is more reliable. Furthermore, the GLASS-AVHRR FVC for July is higher than that for January, while the GEOV1/AVHRR FVC for July is lower than that for January. From that mentioned above, there is a “green up” over Amazon forests during the dry season. Therefore, GLASS-AVHRR FVC is more reliable in terms of seasonality.

Temporal profiles of FVC from the GLASS-AVHRR and GEOV1 FVC products in 1993 over each of the BELMANIP2.1

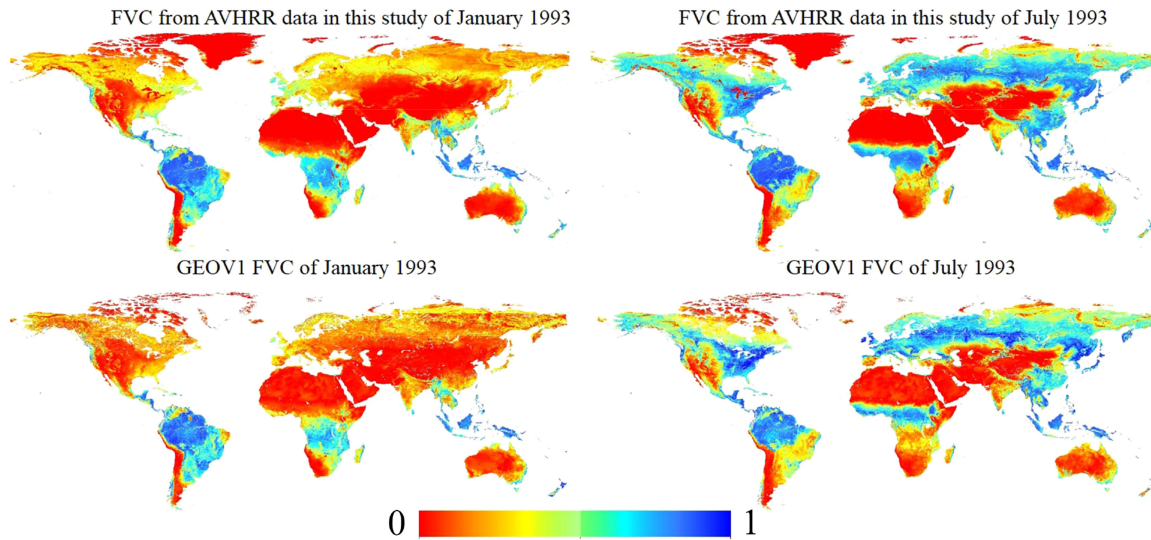


Fig. 7. Monthly averaged global FVC maps generated from the GLASS-AVHRR and GEOV1 FVC products for January and July of 1993. The Antarctic Territories are not included in the map.

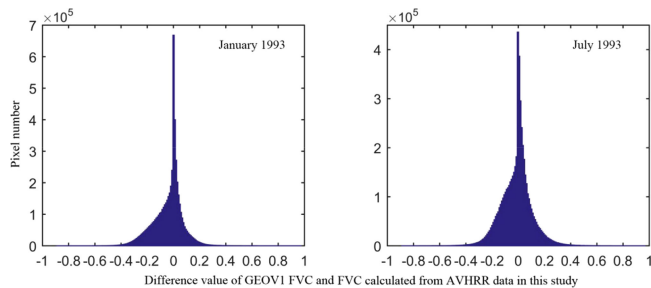


Fig. 8. Histogram of difference values between the GEOV1 and GLASS-AVHRR FVC products for January and July of 1993.

sites were also generated to compare the temporal consistencies and continuities (see Fig. 10). The representative FVC temporal profiles showed the similar seasonal variations between the two FVC products. These temporal profiles could clearly reflect the actual vegetation growth characteristics. The performances of the temporal profiles could confirm the reasonableness of the two FVC products.

Fig. 11 provides several representative FVC temporal profiles from 1981 to 2015 to show the long-term FVC variations. For different vegetation types, GLASS-AVHRR FVC can reflect the growth characteristics and seasonal change properties of vegetation, which confirmed the reasonability of GLASS-AVHRR FVC. Furthermore, none of the temporal profiles have missing data, further confirming the temporal continuity of GLASS-AVHRR FVC.

In total, 44 reference FVC data that were based on field measurements and could represent different vegetation types were used to directly validate the GLASS-AVHRR FVC product, as well as to compare the performance with the GEOV1 FVC product (see Fig. 12). Good agreements between the FVC values from the GLASS-AVHRR FVC product and the reference FVC data were observed, whereas those between the GEOV1 FVC and ground measurements were slightly inferior. The per-

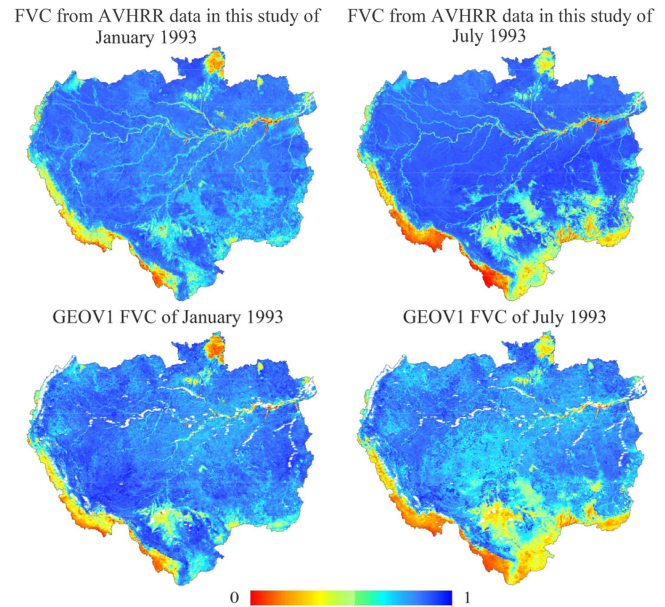


Fig. 9. Monthly averaged GLASS-AVHRR and GEOV1 FVC maps over Amazon River Basin for January and July of 1993.

formance of the GLASS-AVHRR FVC product ( $R^2 = 0.834$ ,  $RMSE = 0.145$ ) was slightly superior to that of the GEOV1 FVC product ( $R^2 = 0.799$ ,  $RMSE = 0.171$ ). Though the number of the validation samples was not large, the validation samples contained various vegetation types and could reflect the performance of the GLASS-AVHRR FVC product to some extent. Therefore, the direct validation results indicated the reliable performance of the GLASS-AVHRR FVC product.

In all, the temporal and spatial comparisons between FVC from the GLASS-AVHRR and GEOV1 FVC products showed the comparable performance of the two products, though certain differences were presented in some specific regions such as the tropical rainforest regions of South America. In addition,



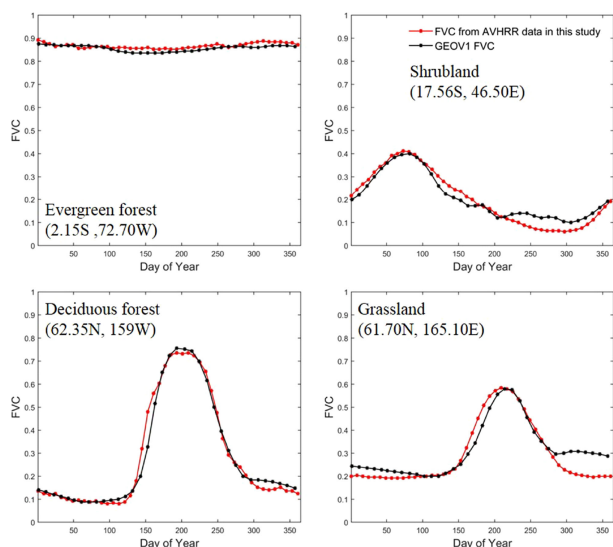


Fig. 10. Temporal profiles of the FVC from the GLASS-AVHRR and GEOV1 FVC products over sampling sites for year 1993.

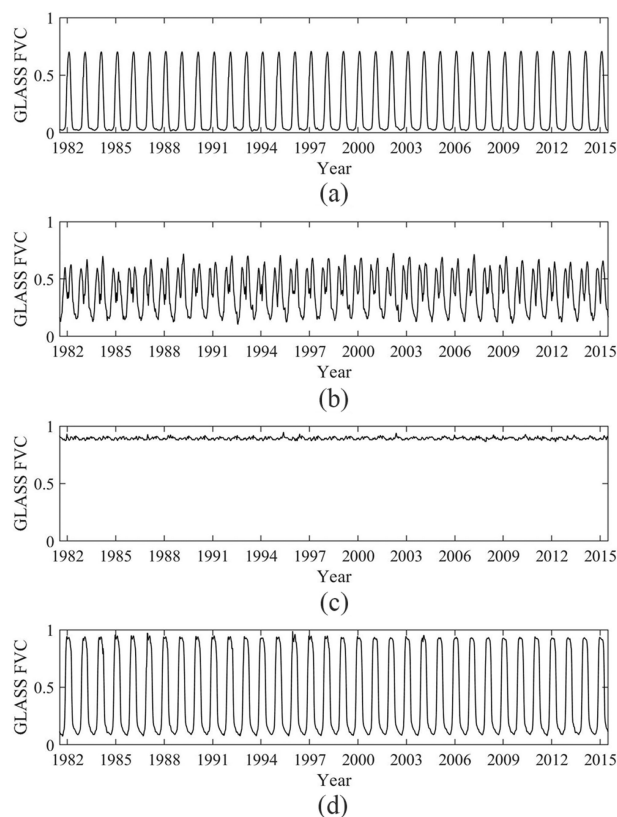


Fig. 11. Temporal profiles of the GLASS-AVHRR FVC over four sites with different vegetation types from 1981 to 2015. (a) Grasslands. (b) Croplands. (c) Evergreen broadleaf forests. (d) Deciduous broadleaf forests.

the GLASS-AVHRR FVC product achieved a slightly better performance based on the direct validation using the field FVC measurements data than the GEOV1 FVC product. Furthermore, the spatial and temporal continuities of the GLASS-AVHRR FVC product were good, and no missing data were observed.

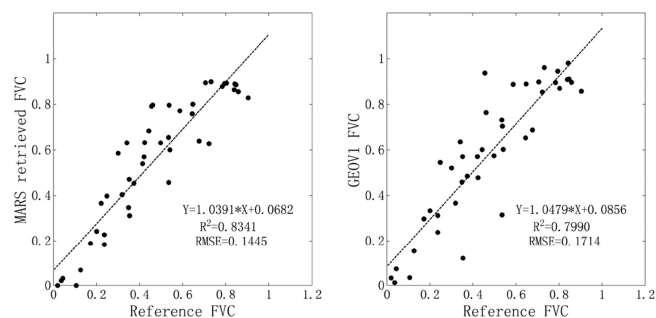


Fig. 12. Comparison of the FVC from the GLASS-AVHRR FVC product (Left), the GEOV1 FVC from VGT data (Right), and the FVC values over the validation sites.

Therefore, all the comparisons further confirmed the reasonability and reliability of the GLASS FVC product.

## V. CONCLUSION

A long-term global GLASS FVC product from MODIS and AVHRR data was introduced in this study. The GLASS-AVHRR FVC algorithm adopted the MARS method with training samples extracted from the GLASS-MODIS FVC product from year 2003 over the global sampling locations. The temporal and spatial consistency between the GLASS-MODIS and GLASS-AVHRR FVC products for year 2013, which could be considered as an independent validation, confirmed the reliability of the GLASS-AVHRR FVC estimation algorithm. Furthermore, the accuracy assessment of the GLASS-AVHRR FVC product using field FVC measurements based reference data indicated that the GLASS-AVHRR FVC algorithm could achieve reliable FVC estimation results when compared to the popular long-term GEOV1 FVC product. In summary, the GLASS FVC product was shown to be reliable and to have good spatial and temporal continuities, thus providing a temporally and spatially consistent, long-time series FVC data set for supporting studies of global climate change and land surface processes. Further work would focus on collecting more field FVC measurements to extensively validate the GLASS FVC product and assessing its performance in climate models, hydrological models, and other related applications. The GLASS FVC product will be released by National Earth System Science Data Sharing Infrastructure of China (<http://www.geodata.cn/thematicView/GLASS.html>) and Global Land Cover Facility (<http://glcf.umd.edu/data/>).

## REFERENCES

- [1] J. L. Roujean and R. Lacaze, "Global mapping of vegetation parameters from POLDER multiangular measurements for studies of surface-atmosphere interactions: A pragmatic method and its validation," *J. Geophys. Res.: Atmospheres*, vol. 107, pp. ACL 6-1-ACL 6-14, Jun. 2002.
- [2] H. Duan *et al.*, "Assessing vegetation dynamics in the Three-North Shelter Forest region of China using AVHRR NDVI data," *Environ. Earth Sci.*, vol. 64, pp. 1011-1020, 2011.
- [3] A. Hampe and R. J. Petit, "Conserving biodiversity under climate change: the rear edge matters," *Ecology Lett.*, vol. 8, pp. 461-467, May 2005.
- [4] T. Wheeler and J. von Braun, "Climate change impacts on global food security," *Science*, vol. 341, pp. 508-513, Aug. 2013.
- [5] G. B. Bonan, "Forests and climate change: Forcings, feedbacks, and the climate benefits of forests," *Science*, vol. 320, pp. 1444-1449, Jun. 2008.

- [6] B. Jiang *et al.*, "Observational evidence for impacts of vegetation change on local surface climate over northern China using the Granger causality test," *J. Geophys. Res.: Biogeosci.*, vol. 120, pp. 1–12, Jan. 2015.
- [7] S. L. Piao *et al.*, "Changes in satellite-derived vegetation growth trend in temperate and boreal Eurasia from 1982 to 2006," *Global Change Biol.*, vol. 17, pp. 3228–3239, Oct. 2011.
- [8] D. Wu *et al.*, "Time-lag effects of global vegetation responses to climate change," *Global Change Biol.*, vol. 21, pp. 3520–3531, 2015.
- [9] F. Baret *et al.*, "GEOV1: LAI and FAPAR essential climate variables and FCOVER global time series capitalizing over existing products. Part 1: Principles of development and production," *Remote Sens. Environ.*, vol. 137, pp. 299–309, 2013.
- [10] A. A. Gitelson *et al.*, "Novel algorithms for remote estimation of vegetation fraction," *Remote Sens. Environ.*, vol. 80, pp. 76–87, Apr. 2002.
- [11] K. Jia *et al.*, "Global land surface fractional vegetation cover estimation using general regression neural networks from MODIS surface reflectance," *IEEE Trans. Geosci. Remote Sens.*, vol. 53, no. 9, pp. 4787–4796, Sep. 2015.
- [12] X. Wang *et al.*, "Fractional vegetation cover estimation method through dynamic Bayesian network combining radiative transfer model and crop growth model," *IEEE Trans. Geosci. Remote Sens.*, vol. 54, no. 12, pp. 7442–7450, Dec. 2016.
- [13] F. Baret *et al.*, "LAI, FAPAR and fCover CYCLOPES global products derived from VEGETATION," *Remote Sens. Environ.*, vol. 110, pp. 275–286, 2007.
- [14] F. Baret *et al.*, "Algorithm theoretical basis document for MERIS top of atmosphere land products (TOS\_VEG)," *ESA AO/1-4233/02/1-LG*, 2006.
- [15] F. J. García-Haro *et al.*, "Operational derivation of vegetation products in the framework of the LSA SAF project," in *Proc. EUMETSAT Meteorological Satellite Conf.*, Dubrovnik, Croatia, 2005, pp. 247–254.
- [16] S. Liang *et al.*, *Advanced Remote Sensing: Terrestrial Information Extraction and Applications*. Oxford, U.K.: Academic, 2012.
- [17] X. Wang *et al.*, "Estimating fractional vegetation cover from landsat-7 ETM+ Reflectance data based on a coupled radiative transfer and crop growth model," *IEEE Trans. Geosci. Remote Sens.*, vol. 55, no. 10, pp. 5539–5546, Oct. 2017.
- [18] H. Godínez-Alvarez *et al.*, "Comparison of three vegetation monitoring methods: Their relative utility for ecological assessment and monitoring," *Ecological Indicators*, vol. 9, pp. 1001–1008, Sep. 2009.
- [19] G. Gutman and A. Ignatov, "The derivation of the green vegetation fraction from NOAA/AVHRR data for use in numerical weather prediction models," *Int. J. Remote Sens.*, vol. 19, pp. 1533–1543, May 1998.
- [20] X. B. Zeng *et al.*, "Derivation and evaluation of global 1-km fractional vegetation cover data for land modeling," *J. Appl. Meteorol.*, vol. 39, pp. 826–839, Jun. 2000.
- [21] X. Zhang *et al.*, "Identification of priority areas for controlling soil erosion," *Catena*, vol. 83, pp. 76–86, 2010.
- [22] K. Jia *et al.*, "Crop classification using multi-configuration SAR data in the north china plain," *Int. J. Remote Sens.*, vol. 33, pp. 170–183, 2012.
- [23] J. M. Bioucas-Dias *et al.*, "Hyperspectral unmixing overview: geometrical, statistical, and sparse Regression-Based approaches," *IEEE J. Sel. Topics Appl. Earth Observ. Remote Sens.*, vol. 5, no. 2, pp. 354–379, Apr. 2012.
- [24] G. Jiapaer *et al.*, "A comparison of methods for estimating fractional vegetation cover in arid regions," *Agricultural Forest Meteorol.*, vol. 151, pp. 1698–1710, 2011.
- [25] J. Xiao and A. Moody, "A comparison of methods for estimating fractional green vegetation cover within a desert-to-upland transition zone in central New Mexico, USA," *Remote Sens. Environ.*, vol. 98, pp. 237–250, 2005.
- [26] K. Jia *et al.*, "Combining estimation of green vegetation fraction in an Arid region from landsat 7 ETM+ Data," *Remote Sens.*, vol. 9, 2017, Art. no. 1121.
- [27] L. Yang *et al.*, "Comparison of four machine learning methods for generating the GLASS fractional vegetation cover product from MODIS data," *Remote Sens.*, vol. 8, 2016, Art. no. 682.
- [28] J. C. Jimenez-Munoz *et al.*, "Comparison between fractional vegetation cover retrievals from vegetation indices and spectral mixture analysis: Case study of PROBA/CHRIS data over an agricultural area," *Sensors*, vol. 9, pp. 768–793, Feb. 2009.
- [29] B. Johnson *et al.*, "Remote sensing of fractional green vegetation cover using Spatially-Interpolated endmembers," *Remote Sens.*, vol. 4, pp. 2619–2634, Sep. 2012.
- [30] B. Wu *et al.*, "Developing method of vegetation fraction estimation by remote sensing for soil loss Equation: A case in the upper basin of miyun reservoir," in *Proc. IEEE Int. Geosci. Remote Sens. Symp.*, 2004, pp. 4352–4355.
- [31] K. Jia *et al.*, "Fractional vegetation cover estimation algorithm for Chinese GF-1 wide field view data," *Remote Sens. Environ.*, vol. 177, pp. 184–191, 2016.
- [32] S. Ahmad *et al.*, "Estimating soil moisture using remote sensing data: A machine learning approach," *Adv. Water Resources*, vol. 33, pp. 69–80, 2010.
- [33] A. Verger *et al.*, "Optimal modalities for radiative transfer-neural network estimation of canopy biophysical characteristics: Evaluation over an agricultural area with CHRIS/PROBA observations," *Remote Sens. Environ.*, vol. 115, pp. 415–426, 2011.
- [34] L. Yang *et al.*, "A robust algorithm for estimating surface fractional vegetation cover from landsat data," *Remote Sens.*, vol. 9, 2017, Art. no. 857.
- [35] F. Camacho *et al.*, "GEOV1: LAI, FAPAR essential climate variables and FCOVER global time series capitalizing over existing products. Part 2: Validation and intercomparison with reference products," *Remote Sens. Environ.*, vol. 137, pp. 310–329, 2013.
- [36] F. J. García-Haro *et al.*, "Inter-comparison of SEVIRI/MSG and MERIS/ENVISAT biophysical products over Europe and Africa," in *Proc. 2nd MERIS(A)TISR User Workshop*, Frascati, Italy, 2008, p. 8.
- [37] X. Mu *et al.*, "Validating GEOV1 fractional vegetation cover derived from Coarse-Resolution remote sensing images over croplands," *IEEE J. Sel. Topics Appl. Earth Observ. Remote Sens.*, vol. 8, no. 2, pp. 439–446, Feb. 2015.
- [38] E. Fillol *et al.*, "Cover fraction estimation from high resolution SPOT HRV&HRG and medium resolution SPOTVEGETATION sensors, validation and comparison over South-West France," in *Proc. 2nd Recent Adv. Quantitative Remote Sens. Symp.*, Valencia, Spain, 2006, pp. 659–663.
- [39] J. Pedelty *et al.*, "Generating a long-term land data record from the AVHRR and MODIS instruments," in *Proc. IEEE Int. Geosci. Remote Sens. Symp.*, Barcelona, Spain, 2007, pp. 1021–1025.
- [40] Z. Xiao *et al.*, "Reconstruction of Long-Term temporally continuous NDVI and surface reflectance from AVHRR data," *IEEE J. Sel. Topics Appl. Earth Observ. Remote Sens.*, vol. 10, no. 12, pp. 5551–5568, Dec. 2017.
- [41] W. J. D. van Leeuwen *et al.*, "MODIS vegetation index compositing approach," *Remote Sens. Environ.*, vol. 69, pp. 264–280, 1999.
- [42] D. Garcia, "Robust smoothing of gridded data in one and higher dimensions with missing values," *Comput. Statist. Data Anal.*, vol. 54, pp. 1167–1178, 2010.
- [43] F. Baret *et al.*, "Evaluation of the representativeness of networks of sites for the global validation and intercomparison of land biophysical products: Proposition of the CEOS-BELMANIP," *IEEE Trans. Geosci. Remote Sens.*, vol. 44, no. 7, pp. 1794–1803, Jul. 2006.
- [44] A. R. Barron and X. Xiao, "Multivariate adaptive regression splines," *Ann. Statist.*, vol. 19, pp. 1–67, 1991.
- [45] J. H. Friedman, "Multivariate adaptive regression splines (with discussion)," *Ann. Statist.*, vol. 19, pp. 102–112, 1991.
- [46] S. L. Liang *et al.*, "Validating MODIS land surface reflectance and albedo products: methods and preliminary results," *Remote Sens. Environ.*, vol. 83, pp. 149–162, Nov. 2002.
- [47] A. R. Huete *et al.*, "Amazon rainforests green-up with sunlight in dry season," *Geophys. Res. Lett.*, vol. 33, 2006, Art. no. L06405.
- [48] S. R. Saleska *et al.*, "Amazon forests green-up during 2005 drought," *Science*, vol. 318, Oct. 26, 2007, Art. no. 612.
- [49] J. Chen *et al.*, "A simple method for reconstructing a high-quality NDVI time-series data set based on the Savitzky-Golay filter," *Remote Sens. Environ.*, vol. 91, pp. 332–344, Jun. 2004.
- [50] J. M. Chen *et al.*, "Locally adjusted cubic-spline capping for reconstructing seasonal trajectories of a satellite-derived surface parameter," *IEEE Trans. Geosci. Remote Sens.*, vol. 44, no. 8, pp. 2230–2238, Aug. 2006.



**Kun Jia** received the B.S. degree in surveying and mapping engineering from Central South University, Changsha, China, in 2006, the Ph.D. degree in cartography and GIS from the Institute of Remote Sensing Applications, Chinese Academy of Sciences, Beijing, China, in 2011.

He is currently an Associate Professor with the State Key Laboratory of Remote Sensing Science and also the Beijing Engineering Research Center for Global Land Remote Sensing Products, Faculty of Geographical Science, Beijing Normal University, Beijing, China. His main research interests include estimation of vegetation parameters, land cover classification, and agriculture monitoring using remote sensing data.



**Linqing Yang** received the B.S. degree in surveying and mapping engineering from Central South University, Changsha, China, in 2015, the M.S. degree in cartography and GIS from Beijing Normal University, Beijing, China, in 2018.

She is currently with the State Key Laboratory of Remote Sensing Science and also the Beijing Engineering Research Center for Global Land Remote Sensing Products, Faculty of Geographical Science, Beijing Normal University, Beijing, China. Her main research interests include estimation of frac-

tional vegetation cover using remote sensing and spatio-temporal analysis of remotely sensed data.



**Shunlin Liang** (M'94–F'13) received the Ph.D. degree from Boston University, Boston, MA, USA.

He is currently a Professor with the Department of Geographical Sciences, University of Maryland, College Park, MD, USA and the School of Remote Sensing Information Engineering, Wuhan University, China. His main research interests focus on estimation of land surface variables from satellite data, earth energy balance, and assessment of environmental changes. He published more than 270 peer-reviewed journal papers, authored the book *Quantitative Remote Sensing of Land Surfaces* (Wiley, 2004), co-authored the book *Global Land Surface Satellite (GLASS) Products: Algorithms, Validation and Analysis* (Springer, 2013), edited the book *Advances in Land Remote Sensing: System, Modeling, Inversion and Application* (Springer, 2008), and co-edited the books *Advanced Remote Sensing: Terrestrial Information Extraction and Applications* (Academic Press, 2012), and *Land Surface Observation, Modeling, Data Assimilation* (World Scientific, 2013).

Dr. Liang was an Associate Editor of the IEEE TRANSACTION ON GEOSCIENCE AND REMOTE SENSING and also a Guest Editor of several remote sensing related journals.



**Zhiqiang Xiao** received the Ph.D. degree in geophysical prospecting and information technology from Central South University, Changsha, China, in 2004.

From 2004 to 2006, he was a Postdoctoral Research Associate with Beijing Normal University, Beijing, China. He is currently with the State Key Laboratory of Remote Sensing Science, Faculty of Geographical Science, Beijing Normal University. His research interests include retrieving land biophysical parameters from remotely sensed data and assimilating radiometric observations into dynamic models.



**Xiang Zhao** received the Ph.D. degree in cartography and GIS from the School of Geography, Beijing Normal University, Beijing, China, in 2006.

He was a Postdoctoral Fellow with the College of Resources Science and Technology, Beijing Normal University during the years 2008–2010. He is now with the State Key Laboratory of Remote Sensing Science, Faculty of Geographical Science, Beijing Normal University. His main research interests focus on high-performance computing system construction and quantitative remote sensing application. He also did some research about long time series remote sensing data trend analysis.



**Yunjun Yao** received the Ph.D. degree from Peking University, Beijing, China, in 2010.

From October 2008 until October 2009, he studied with the Department of Geographical Sciences, University of Maryland, College Park, MD, USA, as a joint Ph.D. student. He is currently with the State Key Laboratory of Remote Sensing Science, Faculty of Geographical Science, Beijing Normal University, Beijing, China. His main research interests include estimation of evapotranspiration and retrieval of surface biophysical parameters by remote sensing.



**Xiaotong Zhang** received the Ph.D. degree in cartography and geographical information science from Wuhan University, Wuhan, China, in 2010.

He was with the Department of Geographical Sciences, University of Maryland, College Park, MD, USA, as a Joint Ph.D. Student. He is currently with the State Key Laboratory of Remote Sensing Science, Faculty of Geographical Science, Beijing Normal University, Beijing, China. His main research interests focus on estimation of land surface radiation components from satellite data, as well as Earth energy balance.



**Bo Jiang** received the B.S. degree from Central South University, Changsha, China, in 2006, the M.S. degree from Beijing Normal University, Beijing, China, in 2009, and the Ph.D. degree from Beijing Normal University in 2012.

From September 2010 until May 2012, she studied with the Department of Geographical Sciences, University of Maryland, USA, as a joint Ph.D. student. She is now with the State Key Laboratory of Remote Sensing Science, Faculty of Geographical Science, Beijing Normal University. Her main research inter-

ests include assessing the impacts of the land cover change on the climate from various observations, and application of remote sensing products.



**Duanyang Liu** received the B.S. degree in remote sensing science and technology from Southwest Jiaotong University, Chengdu, China, in 2017. He is currently working toward the M.S. degree with the State Key Laboratory of Remote Sensing Science, Faculty of Geographical Science, Beijing Normal University, Beijing, China.

His main research interests include estimation of fractional vegetation cover using remote sensing.